On-the-Fly Topological Formation of UAV Swarms

Joseph Camp and Dinesh Rajan
Southern Methodist University, Lyle School of Engineering

With over 600 thousand unmanned aerial vehicles (UAVs) set to take flight within the year, the next wave of autonomous defense applications such as machine-to-machine combat, search and rescue missions, high-definition reconnaissance, and rapid connectivity for disaster recovery requires coordination among UAVs to form three-dimensional (3D) topologies on-the-fly. These topologies depend largely on the intermediate and surrounding geographical features and dynamic spectral activity in a given environment. Fortunately, UAVs are often equipped with a large number of sensors such as Inertial Measurement Units (IMUs), Light Imaging, Detection, and Ranging (LiDAR), or sophisticated 4K or even 3D cameras that can interpret their surroundings. In this extended white paper, we seek to establish a relationship between geographical features observed through images, video, and LiDAR with wireless channel characteristics to establish robust and high-performance communication links for on-the-fly topological formation of UAV swarms. In effect, we propose to build a multi-dimensional, multi-modal data processing framework that includes signal filtering to improve integrity in noisy conditions, extracting information when outliers exist according to contextual factors, and identifying gaps in data to inform future autonomous UAV reconfiguration. Our results (see Fig. 3) indicate that we can predict and verify a doubling in the estimate of the path loss exponent for locations within a few meters from each other, which would dramatically change an optimal swarm topology. However, there are two specific types of uncertainty that could result from these in-flight sensing techniques: propagation prediction and geographical feature extraction. Hence, we consider the topological formation problem in the areas with the greatest level of uncertainty, which requires the understanding of an ideal location at which either supplemental data should be captured or consider the positions at which future swarms can perform these autonomous defense applications.

The main intellectual thrusts of the extended white paper are:

- As a basis for large-scale global analysis, we will leverage 250 million measurements from our Android application and crowdsourcing infrastructure to study the impact of region-based propagation. To do so, we must first understand the imprecision of user equipment as opposed to more advanced instrumentation since mobile phones suffer from such effects as averaging over multiple samples, imprecise quantization, and non-uniform and/or less frequent channel sampling. Then, we will consider the influence of geographical features on propagation and detect inherent outliers from hardware/sensor malfunction that can undermine the wireless channel inference.

- For localized sensing and wireless experimentation, we will leverage hierarchical image processing techniques to detect geographical features with varying heights and visual angles that could be expected with previously-existing images from traffic cameras, satellite imagery, social media uploads, and drones. We then will outfit UAVs with LiDAR and software defined radios to directly measure the wireless propagation characteristics per geographical feature.

- With the global and local feature-based propagation analysis, we will build and on-the-fly topological formation framework for UAV swarms. In particular, we will show a dynamic decision making process based on images, videos, LiDAR, and spectral sensing as nodes are in flight to decide how to best position the swarm in a three-dimensional space to achieve the intended defense goal.

There are three primary outreach opportunities for the project: (*i*) The PI will interface closely with Air Force Research Labs through frequent cross-site visits and mutually-beneficial student internships over the summers of the funding period to strengthen the collaboration. (*ii*) The PIs will teach five hands-on courses to both undergraduate and graduate students across two SMU campuses that will either directly train student researchers or allow them to conduct actual experiments that directly impact the project within the course, and expose all enrolled students to the results of the project. (*iii*) Undergraduates will extensively be involved with the research. Two students have already been working on the image-processing problem via their senior design course, and the PIs will actively recruit exceptional undergraduate students from their hands-on courses for participation in the project.

Key Words: 3D Communication, Topological Swarm Formuation, UAV, Geographical Features, LiDAR, Image Processing, Path Loss, Propagation, Channel Modeling, Signal Filtering, Information Extraction.

On-the-Fly Topological Formation of UAV Swarms

Joseph Camp and Dinesh Rajan
Southern Methodist University, Lyle School of Engineering

Project Description

1 Introduction

The FAA is predicting that 600,000 unmanned aerial vehicles (UAVs) will be in-flight over the coming year [1]. UAV growth will simultaneously pose both threats and opportunities in terms of machine-to-machine combat and offer other autonomous defense applications such as search and rescue missions [2], high-definition reconnaissance [3], and rapid connectivity for disaster recovery [4]. The success of these defense applications will hinge upon the ability to communicate and coordinate between drones across multiple physical altitudes [5, 6] and three-dimensional spaces [7, 8]. However, positioning antennas to communicate in three dimensions is non-trivial since the load carrying capability on a UAV is limited, and the rigid frames often used to increase their load bearing ability block reception on the opposite side of the drone.

Further complicating this issue, the UAV swarm will need to remain connected while traversing across a vast array of environmental contexts, from which there has long been a known relationship between the land use/features and the resulting wireless propagation [9, 10]. For example, many works have used detailed measurements from a particular area and/or a particular piece of hardware [11–14] to create path loss models for specific region types (*e.g.*, urban, suburban, or rural). The goals of these studies were to produce models that were independent of exact physical locations and broadly applicable to any environment. Conversely, Radio Mobile [15] is a widely-used, open-source tool used by many in the cellular industry, but the propagation prediction depends almost entirely on elevation data without regard for buildings, trees, and other above-land structures and land use data.

Fortunately, UAVs have a number of sensors such as Inertial Measurement Units (IMUs), Light Imaging, Detection, and Ranging (LiDAR), or sophisticated 4K or even 3D cameras that can offer hints as to the surrounding geographical features and potentially which general direction to direct transmissions. In this extended white paper, we seek to establish a relationship between geographical features observed through images, video, and LiDAR with wireless channel characteristics to establish robust and high-performance communication links for on-the-fly topological formation of UAV swarms. In effect, we propose to build a multi-dimensional, multi-modal data processing framework that includes signal filtering to improve integrity in noisy conditions, extracting information when outliers exist according to contextual factors, and identifying gaps in data to inform future autonomous UAV reconfiguration. Our results (see Fig. 3) indicate that we can predict and verify a doubling in the estimate of the path loss exponent for locations within a few meters from each other, which would dramatically change an optimal swarm topology. However, there are two specific types of uncertainty that could result from these in-flight sensing techniques: propagation prediction and geographical feature extraction. Hence, we consider the topological formation problem in the areas with the greatest level of uncertainty, which requires the understanding of an ideal location at which either supplemental data should be captured or consider the positions at which future swarms can perform these autonomous defense applications. To do so, our project consists of the following research thrusts:

- As a basis for large-scale global analysis, we will leverage 250 million measurements from our Android application and crowdsourcing infrastructure to study the impact of region-based propagation. To do so, we must first understand the imprecision of user equipment as opposed to more advanced instrumentation since mobile phones suffer from such effects as averaging over multiple samples, imprecise quantization, and non-uniform and/or less frequent channel sampling. Then, we will consider the influence of geographical features on propagation and detect inherent outliers from hardware/sensor malfunction that can undermine the wireless channel inference.

- For localized sensing and wireless experimentation, we will leverage hierarchical image processing techniques to detect geographical features with varying heights and visual angles that could be expected with previously-existing images from traffic cameras, satellite imagery, social media uploads,

and drones. We then will outfit UAVs with LiDAR and software defined radios to directly measure the wireless propagation characteristics per geographical feature.

- With the global and local feature-based propagation analysis, we will build and on-the-fly topological formation framework for UAV swarms. In particular, we will show a dynamic decision making process based on images, videos, LiDAR, and spectral sensing as nodes are in flight to decide how to best position the swarm in a three-dimensional space to achieve the intended defense goal.

The underlying theme across all of these research thrusts is the ability to extract useful information from large-scale, multi-modal data. In Research Task 1, we focus primarily on signal quality data and study the wireless behavior on a global or regional area by statistically considering the aggregation of geographical features. This task will also require determining appropriate data distributions and leveraging it to identify outliers. In Research Task 2, we process 2-D and 3-D visual and LiDAR data to extract a individual geographical feature vectors that can provide concise and quantitative information about the role of wireless in and around these particular objects. In the final Research Task, we leverage these two knowledge bases to understand the correlations in antenna orientation and relative positioning of the drones to build multi-dimensional UAV topologies on the fly.

2 Research Task 1: Global Wireless Channel Inference and Outlier Detection

In seeking to build on-the-fly topologies with UAVs, we must first understand the relationship between the at-large geographical features in a region with the wireless propagation. To generate a very large data set to do so, we have built a crowdsourcing framework that has captured 250 million signal measurements around the world. In this section, we will describe the three research steps to leverage this database to understand propagation characteristics on a global scale. First, we seek to understand how precisely we can model wireless channels with the crowd's devices (mobile phones) as opposed to advanced test equipment. Second, since mobile phones are subject to greater levels of noise and inaccuracy, we detect outliers that will manifest from user equipment, especially within the same geographical features to improve our iterative analysis. Third, we seek to improve wireless channel inference by leveraging geographical features in our propagation model. The global or regional geographical feature set could be constructed via the use of LiDAR or satellite imagery. While the use of expensive data gathering mechanism such as LiDAR can provide accurate spatial data on certain geographical features such as elevation, the acquisition cost can be prohibitive. However, the abundance of open-source [16], visible terrestrial imagery data along with the increasing use of drones can help to fill the gaps in data availability.

2.1 Background and Related Work

There have been a number of works that leveraged the value of crowdsourcing for applications such as studying network topology [17], performing real-time network adaptation [18], characterizing Internet traffic [19], detecting network events [20], fingerprinting and georeferencing [21], assessing the quality of user experience [22], and understanding network neutrality [23]. As mentioned, we feel that crowdsourcing could prevent many costly iterations of drivetesting for wireless propagation characteristics for many cellular technologies, frequency bands, and even tower settings [24]. In fact, LTE Release 10 of the 3GPP Technical Standard 37.320 has already worked to minimize drivetesting and improve self-optimization of coverage and handover [25–28].

Small-Scale Fading. Small-scale fading occurs when multiple paths are taken for the same transmitted symbol resulting in differing arrival times at the intended receiver. A number of well-known distributions have been used to model small-scale fading effects such as Rician, Rayleigh, log-normal, and Nakagami. While Rayleigh focuses on characterizing non-line-of-sight paths, Rician characterizes a mixture of both line-of-sight and non-line-of-sight paths. We use the Nakagami distribution since it can model both Rayleigh and Rician distributions [29, 30]. The Nakagami probability density function (pdf) or m-distribution of the received signal envelope, r, has been defined below, where Γ refers to the Gamma function:

$$f(r) = \frac{(2m^m r^(2m-1))}{(\Gamma(m)\Omega^m)} \exp(-\frac{m}{\Omega} r^2) \tag{1}$$

Here, Ω is the local power (signal variance), $\Omega = E[X^2]$, and the m-parameter defines the severity of fading:

$$m = \frac{E^2[X^2]}{Var[X^2]}, \qquad m \geq \frac{1}{2} \tag{2}$$

Having the knowledge of the m value can be used in a variety of applications, such as development of cellular access mechanisms, transmission diversity and combining techniques, adaptive modulation schemes, modeling and analysis of interference and outage probabilities, and design and simulation of adaptive antennas systems. In most of these applications, m is quantized to an integer value to simplify the analysis [31–33].

Large-Scale Fading. Large-scale fading refers to the average attenuation in a given environment due to transmission through and around obstacles for a given distance [34]. There are three main types of models to calculate the channel characteristics in terms of large-scale fading: mathematical, physical, and empirical. Physical models, such as Friis equation [35] and ray tracing [36,37], need very detailed information about the environment and have high computational complexity, but offer very high accuracy. Empirical models, such as Okumura [38] and Hata [12], use simple equations and less site specific information, but the accuracy is not very high. Mathematical models can be used alongside empirical models to increase the accuracy of the prediction while keeping this complexity relatively low. Examples of these works include prediction of path loss in a microcell [39], rural area [40], suburban area [41], urban area [42], and indoors [43]. As has long been shown, the accuracy of the predicted channel characteristics is related to the degree to which obstructions of a cell site, such as buildings and trees, are included in the analysis [44]. Tree density and type and land use have been used from satellite imagery [39,45], having similarities to our work. However, we seek to use video and multiple vantage points from drones to improve the precision of the feature detection in the following section.

Frequently, a log-distance model is used to characterize large-scale fading in which signal strengths and distances are obtained between the transmitter and receiver and can be represented by:

$$PL_d(\text{in dB}) = PL_0 + 10\gamma \log \frac{d}{d_0} + X_g \tag{3}$$

Here, PL_d, represents the total path loss in dB at a given distance d between the transmitter and receiver, PL_0 represents the power received at the reference distance d_0, γ is the path loss exponent, and X_g is a normally-distributed, zero-mean random variable which shows the flat-fading attenuation. The path loss exponent γ varies due to the environmental type from 2 in free space to 6 in indoor environments. Some typical cellular γ values are 2.7-3.5 in typical urban scenarios and 3-5 in heavily shadowed urban environments.

2.2 Proposed Work

To visualize the issues involved with using mobile phones in place of drive testing equipment for channel characterization, we have depicted the process of data collection and the proposed post-processing steps in Fig. 1(a). We start with raw signal strength measurements from a Rohde & Schwarz TSMW Channel Scanner, a phone equipped with Rohde & Schwarz firmware, and a regular phone equipped with our WiEye spectrum analyzer. At the API level, we have developed an Android application called WiEye, which can be used by users globally as an economical spectrum analyzer. At the firmware level, we collect signal quality directly from the hardware via Qualipoc application from Rohde & Schwarz. Collected data will be passed to the outlier removal module to remove measurements that lack information about the location or transmitter characteristics. The outlier removal module will progressively improve after considering and isolating geographical features in the next sub-task. Since it has been shown that the network performance can vary per sector, we categorize data with respect to the base station sector, which is transmitting the received signal. We then will process per sector data from the channel scanner to resemble data that would come from a mobile phone by imposing similar effects as the mobile phone imperfections: averaging, uniformly and non uniformly downsampling over time and space, and quantization. After each effect is applied, we compare the results of the new data set in terms of fading with a reference channel characteristic. The reference value is obtained by considering all measurements in the channel scanner data set.

After evaluating the accuracy of phone measurements, we will generate radio environment maps based on UE measurements to predict the performance of the areas with low or no number of measurements. To

do so we overlay a map of the geographical features of the environment over the estimation of the network performance. Lastly, we use Artificial Neural Network (ANN) along with the geographical features and obtained Key Performance Indicator (KPI) from measurements to predict the network performance.

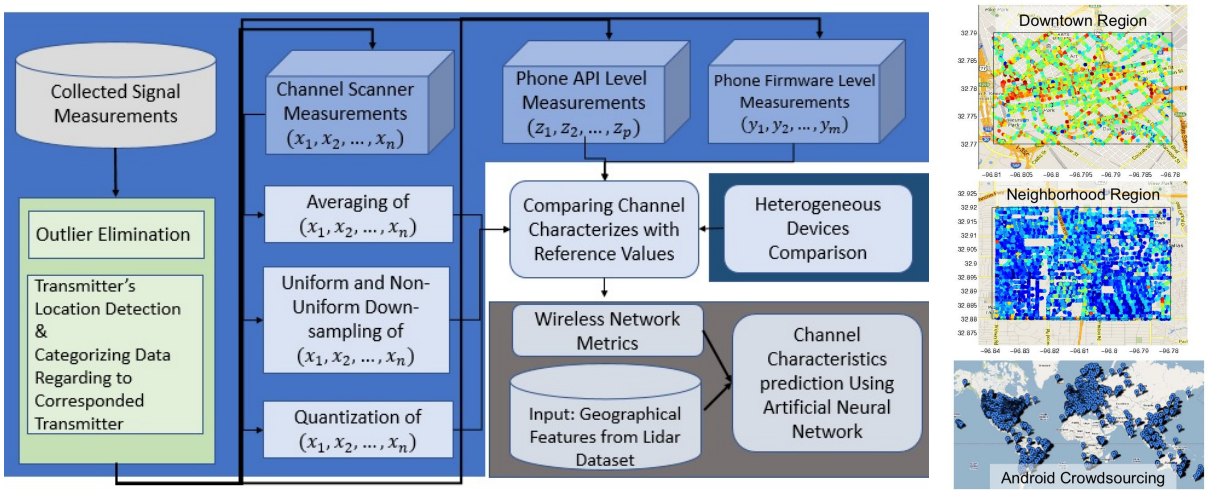

(a) Task 1 Overview. (b) Data Sets.

Figure 1: Mobile phone based channel inference (left) and local and global data sets (right).

Use of Mobile Phones. We will evaluate the quality of the collected data by mobile phones to calculate channel characteristics in terms of small- and large-scale fading, respectively. In our work, we will use the Nakagami shape factor and path loss exponent of the log-distance model to represent the channel characteristics. When used as measurement devices for received signal strength, mobile phone data is subject to averaging, quantization, and non-uniform downsampling effects not present when using more sophisticated and dedicated drivetesting equipment (*e.g.*, TSMW). In our initial analysis, we have collected in-field local measurements in three different region types: downtown, multi-family, and single-family residential environments. In performing these measurements, we have used a Rohde & Schwarz TSMW Channel Scanner alongside two Android Samsung Galaxy S5 mobile phones on the roof a vehicle. The phones are equipped with our spectrum analyzer and the customized application (Qualipoc) from Rohde & Schwarz, respectively.

Fig. 7(b) depicts 6.7 million measurements in both the downtown and suburban regions. The lighter shaded dots correspond to measurements with higher Received Signal Strength Indicator (RSSI) and the darker shaded dots correspond to measurements with lower RSSI. In the suburban region, we are not able to cover several small areas due to gated communities, resulting in the areas lacking measurements seen in the figure. Lastly, we have an Android based application called WiEye, which has collected over 250 million crowdsourced measurements globally since April of 2011 (the spatial data footprint is also shown in Fig. 7(b)). We will increasingly rely upon the Android data set through the course of the project as we are able to fully quantify the relationship between advanced drive testing equipment and crowdsourced mobile phone data.

Representation of Received Signal Level in Phone. Each cellular measurement contains a received signal level field reported as RSSI with GSM networks and Reference Signal Receive Power (RSRP) in LTE networks. While we now obtain received signal level readings in terms of dBm with GSM and LTE networks, most of our measurements were taken when the API reported received signal level in terms of Arbitrary Strength Units (ASU). In fact, while we have 3.6M LTE measurements, 1.7M measurements are reporting a dBm measurement at the maximum value. Hence, we currently have only 1.9M usable LTE measurements as opposed to over 110M usable GSM measurements (there are approximately 140M WiFi signal quality measurements). The Android API quantizes the obtained RSSI values into ASU units: $P_{rx}(dBm) = 2 * P_{rx}(ASU) - 113$ where $P_{rx}(ASU) \in [0, 31]$. Also, the valid range of the reported ASU in an LTE network is 0 to 97, from which the range of 1 to 96 are mapped to $ASU141dBm < ASU140$. Here,

0 and 97 are corresponding to RSRP below or above -140 and -44 dBm, respectively.

We consider two ultimate ranges (0, 31) and (0, 97), unusable since they correspond to SNR in an unlimited range; *e.g.* an ASU value of 31 includes any RSSI value above -51 dBm. Not including these measurements, however, clips the natural distribution of RSSI readings at locations with measurements near the quantization limits. The lower and upper bounds set by omitting measurements where $P_{rx}(ASU) = 31$ and $P_{rx}(ASU) = 0$, respectively, can bias the average RSSI at certain distances from the tower. Distances closer to the tower that generally have higher RSSI measurements near the upper bound may have a lowered average RSSI. Conversely, distances farther from that tower that generally have lower RSSI measurements near the lower bound may have a heightened average RSSI. The bias in the movement of average RSSI near the boundaries could end up changing (likely reducing) the value of the obtained path loss exponent.

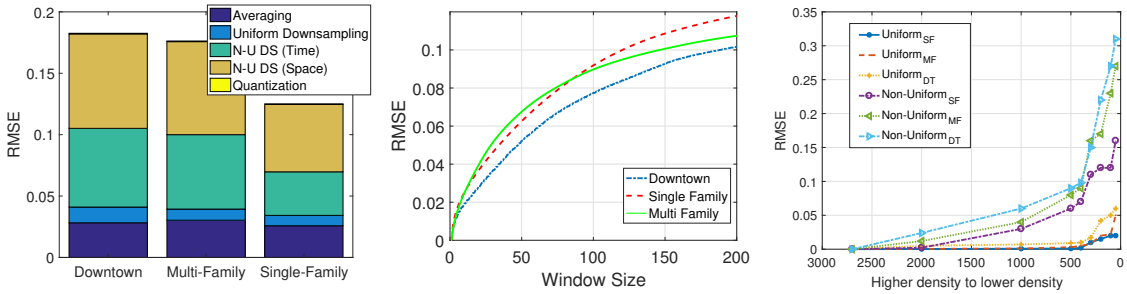

(a) All Factors. (b) Averaging. (c) Downsampling.

Figure 2: Mobile phone challenges of quantization, averaging, and downsampling in crowdsourcing channels.

We depict the impact of the four mobile phone factors (averaging, uniform and non-uniform downsampling in space and time, and quantization) on the calculation of path loss exponent (γ) in Fig. 2(a). Here, we run the algorithm described in Fig. 1(a) on the collected data by the selected cell towers in the previous section. We apply the averaging on signal samples which are quantized already. Then, we downsampled (uniformly and non-uniformly in time and space) from the sampled which are already averaged and quantized. The bar chart shows the relative impact of jointly consideration the mobile phone imperfections on the channel characteristics estimation in terms of γ. There are two interesting findings from these results: *(i)* either form of non-uniformly downsampling is clearly the most dominant effects considered when predicting the path loss exponent, and *(ii)* the two non-uniform downsampling techniques (time and space) have approximately equivalent performance (despite the noise of non-uniformly downsampling noted earlier). The latter finding offers great hope for crowdsourced data sets to be influential in characterizing the path loss characteristics of an environment.

Averaging of Received Signal Power. Network interfaces often use some form of hysteresis to suppress sudden fluctuations in channel state that might lead to overcompensation in adaptive protocols. Many times this hysteresis is performed by averaging multiple received signal qualities before reporting it to the higher layers and/or the user. Each device uses its own policy (often proprietary) to take a specific number of samples over a certain period of time. A phone in an LTE network is required to measure the RSRP and Reference Signal Received Quality (RSRQ) of the serving cell and neighboring cells continuously for handover and cell selection purposes. The measurement should be performed at least every Discontinuous Reception (DRX) cycle to see if the cell selection criteria is satisfied [**?**]. To do so, a filter is applied on the RSRP and RSRQ of the serving cell to continually track the quality of the received signal. Within the set of measurements used for the filtering, two measurements shall be spaced by no longer than half of the DRX cycle [**?**]. On the other hand, a mobile phone receives multiple resource elements and measures the average power of resource elements.

We attempt to empirically find the average window size used for a Samsung Galaxy S5 phone. To do so, we compared the calculated γ parameter obtained by the mobile phone and corresponding channel scanner data set obtained from 8 different cellular base stations. Meanwhile, we considered a similar rolling-average window size from 0.25 to 6 seconds using channel scanner signal strength data. In Fig. 2(b), we depict the variation of the γ parameter by changing the averaging window from 0.25 to 6s on the collected measurements by the channel scanner, which corresponds to a window size of 0 to 200 samples. We averaged the RMSE

corresponding to each window size over multiple base stations in each region. As depicted, by increasing the averaging window size, the maximum error in three regions is about 0.1. Reconsidering the results from Fig. 2(a), as we study LTE devices that have a lower window size, we expect that the averaging effect will reduce to be a less dominant effect as compared to the downsampling effect, which will be critical in crowdsourcing.

Uniform and Non-Uniform Downsampling. When crowdsourcing signal quality from mobile phones, there is a limitation on the number and contiguity of a single user's measurements due to data usage and battery consumption limitations. Even without such a limitation, there is a far more strict limit on the number of measurements possible by the phone versus the channel scanner. For example, the maximum sampling rate of the TSMW is 500 samples per second versus 1 sample per second using WiEye with the Samsung Galaxy S5. In fact, it is reasonable to assume that measurements from a particular region are not coming from a single user, but from multiple users. We study the impact of differing numbers of measurements on the path loss prediction by calculating the γ parameter from a particular sector of a base station in three regions by applying uniformly and spatial non-uniformly downsampling. For non-uniform spatial downsampling, we chose the measurements based on three clusters which are randomly distributed over the region. Then, we gradually increase the number of the selected measurements in each cluster. Lastly, we compare the path loss exponent of the aggregated samples from three clusters with the reference γ. Fig. 2(c) shows the role of the uniformly downsampling as opposed to spatial non-uniformly downsampling in three regions.

Key Research Questions: *How close will the estimate of channel characteristics (large and small scale fading) computed from the mobile phone samples m_Y be to that of the estimate of m and γ from the channel scanner samples m_X? Additionally, as the mobile phone preserves energy and/or data usage, how would the m and γ parameters further diverge when the sampling interval becomes significantly larger?*

Outlier Detection in Crowdsourced Channel Measurements. We have previously built outlier detection algorithms for rate adaptation protocols [46]. In particular, we have used a linear-regression based model from [47] to represent the matrix $\mathbf{W} \in \mathbb{R}^{m \times l}$ with parameter α controlling $Tr(\mathbf{W}^\top \mathbf{W})$, the regularization weighting term, to avoid over-fitting:

$$\min_{\mathbf{W}} \quad \|\mathbf{W}^\top \mathbf{X} - \mathbf{Y}\|_F^2 + \alpha Tr(\mathbf{W}^\top \mathbf{W}). \tag{4}$$

Here, let $\mathbf{X} = [\mathbf{x}'_1, \mathbf{x}'_2, ..., \mathbf{x}'_n]$ represents the given data attribute vector (based on geographical features), where n represents the number of data points, and $\mathbf{Y} \in \mathbb{R}^{l \times n}$ represent the optimum class indicator matrix, where l is the number of classes. These classes were originally targeted for transmission rates that were optimal for the given context. However, for this project, a quantized form of channel characteristic parameters would form the classes. For example, a range of path loss values or Nakagami m parameters which form from the data set.

Let $\mathbf{B} = \mathbf{W}^\top \mathbf{X} + \mathbf{Y} + \Omega$ for a residual matrix size $n \times l$ to find the outlier in the data set, and Ω represents the random error matrix from the linear regression model. The outlier detection problem can therefore be formulated according to:

$$\min_{\mathbf{W},\mathbf{B}} \quad \|\mathbf{W}^\top \mathbf{X} - \mathbf{B}^\top - \mathbf{Y}\|_F^2 + \alpha Tr(\mathbf{W}^\top \mathbf{W}) + \beta \|\mathbf{B}\|_{2,1}, \tag{5}$$

where $\|\mathbf{B}\|_{2,1}$ is the $\ell_{2,1}$-norm of $\mathbf{B}$, which is defined as follows [48],

$$\|\mathbf{B}\|_{2,1} = \sum_{i=1}^{n} \sqrt{\sum_{j=1}^{l} \mathbf{B}^2(i,j)} = \sum_{i=1}^{n} \|\mathbf{B}(i,:)\|_2. \tag{6}$$

Here, $\ell_{2,1}$-norm on $\mathbf{B}$ serves the purpose of ensuring that $\mathbf{B}$ is sparse and to not form a trivial estimate for $\mathbf{B} = \mathbf{Y}^\top$. We have shown this problem to be jointly convex for $\mathbf{W}$ and $\mathbf{B}$ [46]. However, as we refine the role of geographical features in channel inference, we hypothesize that a better estimate of $\mathbf{W}$ (and corresponding optimal value of $\mathbf{B}$) will form for a given environmental feature or set of features, thereby increasing the confidence of whether a given data point is an outlier. To investigate the validity of this hypothesis, we will restrict the selection of $\mathbf{X}$ according to the specific geographical feature or set of geographical features from which the measurement was taken. We now discuss how to define such a region.

Geographical Feature Influence on Propagation. Previously, we have either restricted our analysis to a particular base station or considered all base stations in an arbitrarily defined region. However, such an approach does not take into account the long understood relationship between wireless propagation and obstacles in the environment and letting that relationship define the region over which to perform wireless channel characterization. Hence, we now establish a mechanism to predict the wireless channel propagation by exploiting the geographical features, such as the features of the buildings and trees in the studied region, since they are the main reason of diffraction and scattering of the transmitted signals. In this section, we will use Light Detection and Ranging (LiDAR) data to represent these land features. However, such an approach will not scale to any environment due to the cost of LiDAR where it exists and the lack of LiDAR in many international regions. Hence, in the subsequent section, we will use image processing techniques from crowdsourced pictures and videos (*e.g.*, from drones) to capture the environmental features. In either case, our goal is to develop an empirically-driven relationship between the crowdsourced propagation data and the geographical features. To do so, we need to select a set of features as inputs to a machine learning mechanism through the training and learning phases. LiDAR uses lasers to detect distances and scattering along the Earth's surface. We use the LiDAR Analyst in ArcMap to analyze the LAS files. The processed files consist of the following land features for: *(i)* trees - height, crown area and diameter, trunk diameter, and tree type, and *(ii)* buildings - height, area, and roof type.

In our initial analysis on the role of geographical features, we use a fixed-sized square that moves through a particular region. We then select the square with the minimum and maximum path loss exponent to examine the geographical features that are contributing to the propagation differences. The center of Fig. 3 depicts the captured measurements in a Dallas-based, multi-family residential area with a base station located in the top-center of the lower white square and depicted by a red dot. The area is covered by a combination of buildings with at least two stories and trees. The level of the received signal is depicted by a darker color (blue) to indicate a lower RSSI level versus a lighter color (yellow) to indicate a higher RSSI level. The moving square for analysis covers a region of 300 m square. Considering the squares with at least 500 measurements, we consider 41 different non-overlapping squares. The left and right of Fig. 3 shows the area with minimum and maximum path loss exponents, respectively. The minimum path loss exponent (1.6) occurs in the square with the tallest building (9.1 m) in the area, somewhat counter-intuitively. However, since these measurements were all outdoor, the received signal strengths were all either line-of-sight or with strong reflections off of hard surfaces as opposed to inside or behind the building. In contrast, the maximum path loss exponent (3.1) occurred in a region with shorter buildings that do not completely block the signal on the back side of the buildings. Note that the starkest difference between the path loss exponent over this entire region occurs between adjacent squares, essentially doubling the path loss exponent by simply crossing the street.

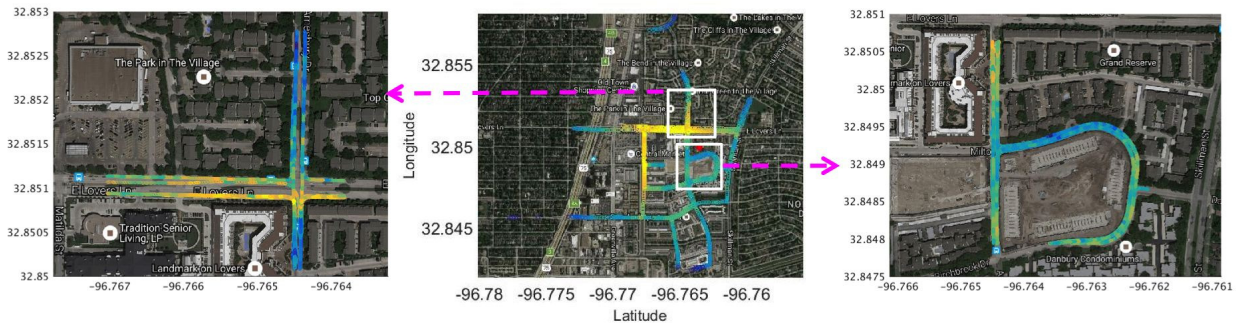

Figure 3: Minimum (left) and maximum (right) path loss exponent in a multi-family residential area.

Similarly, Fig. 4 shows the collected data by a base station in downtown Dallas. The left and right portion of the figures depict the squares with the minimum (1.7) and maximum (2.5) path loss exponents, respectively, among 25 qualified squares. The base station is located in the top-left of the center image and depicted by a red dot. Table 1 shows the mean RSSI, mean and standard deviation of the building and tree heights, and the resulting path loss exponents. The heights of the buildings in the minimum path loss

exponent square are greater (by 3 m) with greater diversity in height (by 3 m) than the maximum path loss exponent square, serving as many opportunities for the signal from the base station to be reflected. While having lower building heights, the maximum path loss exponent square has measurements that are almost entirely behind a building with respect to the direct path to the base station, but the building is short enough to not completely block the signal, causing a net effect of higher levels of attenuation.

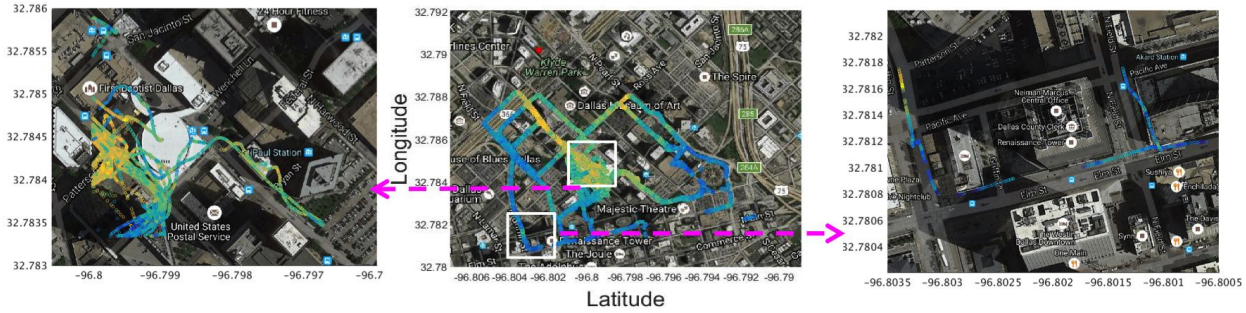

Figure 4: Minimum (left) and maximum (right) path loss exponent in a downtown Dallas area.

Table 1: Geographical feature properties in the downtown area and resulting path loss exponents.

Tile	Ave-RSSI (dBm)	Path Loss Exponent	Ave-BH	STD of BH	Ave-TH	STD of TH
$min\gamma$	1.7	-50	8.5	4.1	10.5	2.3
$max\gamma$	2.5	-77	5.6	0.8	13.4	5.2

We then examine a mixed-use urban area in Dallas where there is a combination of commercial entities, single-family residential neighborhoods, and multi-family residential structures, depicted in Fig. 5. The minimum (2.2) and maximum (3.6) path loss exponent is pictured left and right, respectively, out of 110 qualified squares. The minimum occurs where there is an absence of building structures (due to a highway intersection) along the path between the cell tower (pictured in red near the center of the picture) and the receiver locations. The maximum path loss exponent occurs in a single-family residential area as an example of a homogeneous set of geographical features. It will be these broad areas of consistent geographical features that will form training sets for us to understand each geographical feature's contribution.

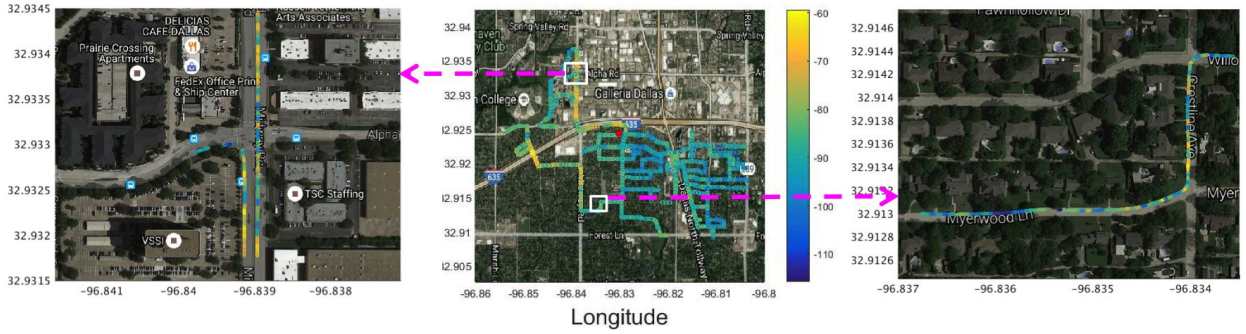

Figure 5: Minimum (left) and maximum (right) path loss exponent in a mixed-use urban area.

Lastly, we consider the correlation between the path loss exponent value and the geographical features of building and tree heights among the three examined regions of Dallas. In all three cases, the mean RSSI is strongly negatively correlated with the path loss exponent, meaning there are rarely cases where strong received signals correspond to poor propagation environments or vice versa. Surprisingly, in the multi-family residential environment and downtown, the building height is also negatively correlated with the path loss exponent. These apartment and skyscraper structures consist of far more metal and concrete to block signals from propagating through these structures and often produce strong reflections. In contrast, the mixed-use urban area had a large number of single-family homes that flipped the correlation to be positive.

Table 2: The correlation between the geographical features and path loss exponent.

Area Type	Mean-RSSI	Mean-Blg. Ht.	STD-Blg. Ht.	Mean-Tree Ht.	STD-Tree Ht.
Multi-Family Res.	-0.82	-0.3	0.2	0.2	0.2
Downtown	-0.8	-0.3	0.2	0.1	0.4
Mixed Urban	-0.8	0.23	0.24	0.23	0.2

The area of the buildings and trees, as well as the small-scale fading, will be considered using a similar approach. However, the most important scientific issue is understanding the role of a particular geographical feature on the resulting path loss. To do so, we use the relationship between the received signal level and foliage and buildings surrounding the location of the receiver to build an ANN model to predict the path loss exponent of a region with no enough number of measurements. We provide a two-layer map, with a specific grid size. One map consists of the geographical features of a region (grid) and the other one contains the corresponding performance of the network in terms of path loss exponent. We train the ANN model using geographical features and path loss exponents as the input and output of the model, respectively. After building the model, we can predict the channel characteristic of unknown areas with no in-field measurements.

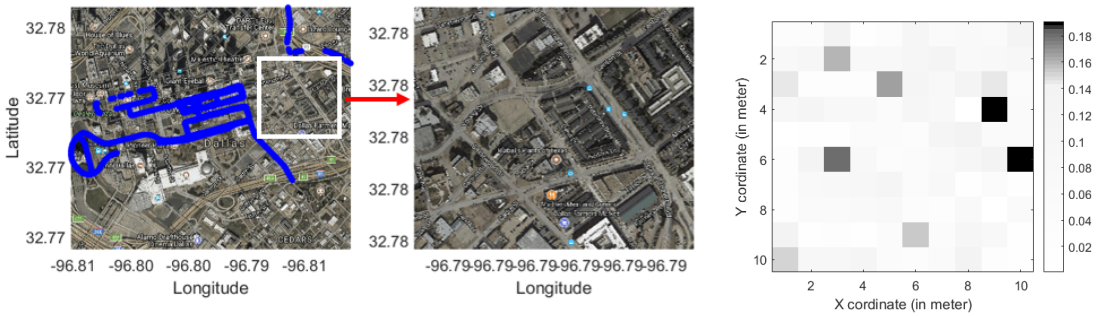

(a) Adjacent sub-region.

(b) Absolute Error.

Figure 6: Blind inference approach to understanding geographical features.

As we build an expected path loss exponent for each grid, we could consider a given area with a known geographical feature set and all the resulting path loss exponents (see Fig. 6(a), left, which represents a set of known features and corresponding γ). Then, we emulate a crowdsourcing context in which there is lack of measurements from users in a certain area surrounded by the area with an adequate number of measurements. We could then predict the actual loss from a base station to a given receiver location by weighting the propagation path according to the path loss exponent and the percentage of distance along the path that the geographical feature consumes. Fig. 6(b) shows the channel characteristic prediction results, which the absolute error of the majority of the prediction error is below 0.1.

Key Research Step: *Finding and defining these homogeneous regions will be a key step in the analysis. Also, to increase the accuracy of the model we need to find the most relevant factor from geographical features to the path loss. Furthermore, we need to figure out how to select the geographical features between the transmitter and receiver to increase the correlation between these factors and output of the model. Initially, within the context of Dallas, we can rely on planned communities (i.e., neighborhoods) of different age, resulting in differing tree heights and densities. Additionally, there are portions of the commercial or multi-family residential areas that have similar building characteristics (e.g., height, materials, and area). The LiDAR data can be overlaid on the region's signal strength measurements. However, limiting our study to Dallas would have the severe drawback of only certain types of trees and buildings and relatively flat elevation. Hence, the image-based extraction of geographical features (see Section 3) is critical to fully leverage our crowdsourced wireless signal measurements to find large homogeneous feature sets globally that have different geographical characteristics than Dallas.*

3 Research Task 2: Local Image- and LiDAR-based Geographical Feature Isolation

The previous section worked with global or regional LiDAR or satellite data to process geographical features as a statistical collection and relate those feature sets to wireless propagation. In this section, we attempt to use local images and LiDAR sensing to isolate specific geographical features and build an intuition for their individual role on propagation.

3.1 Related Work

There have been many works that identify buildings from a single intensity aerial image [49, 50]. Video has been used with a point cloud to also model buildings and other structures [51], even combining with LiDAR data [52]. Other works that combined pictures from multiple sources such as Google Street View and aerial imagery to detect and catalog trees [53]. However, the primary concern in this work was identifying tree species as opposed to tree height, density, and canopy features, which is an important concern with wireless propagation. Similarly, [54–56] uses a categorization of image data into coarse land-use categories and uses machine learning to predict the path loss in each of those areas.

3.2 Proposed Work

Data Fusion. The plethora of open-source image data that is available consists of data captured at different times of the day and year, each at different illumination levels using different resolution cameras (*e.g.*, via satellites, drones, airplanes, and high rise buildings). Given the variety of different sources from which data is available, an adaptive and intelligent fusion algorithm will be developed. The proposed unified algorithm will have 3 primary attributes: *(i)* improve spatial resolution using digital super-resolution methods [57, 58], *(ii)* remove noisy outliers (caused, for example, by erroneous GPS coordinates for a given data), and *(iii)* extract 3D structural information using either data from cameras or multiple viewpoints or from video data from a single moving platform (such as a drone), using robust camera calibration techniques [59]. The fundamental idea is to use multi-dimensional data from various sources to extract actionable information in a lower-dimensional space.

The forward imaging model that represents the image capture mechanism can be converted from a linear convolutional model and written in matrix-vector notation as follows:

$$\mathbf{g}_i = \mathbf{DHM}\mathbf{f}_{c,v} + \mathbf{n}_i \tag{7}$$

In (7), c and v represent the location and field-of-view (FOV) of the image frame being captured, $\mathbf{f}$ and $\mathbf{g}$ represent, respectively, the true image data and captured image, $\mathbf{D}$ represents the downsampling matrix, $\mathbf{H}$ represents the unified convolutional operation, and $\mathbf{M}$ represents the motion and warping operation. Also, in (7), the 2-dimensional image data are converted to 1-dimensional vectors for convenience and index i represents a single index into a lexicographical and temporally-ordered frame from the various imagers available at location c. In this project, we will use blind estimation techniques to estimate $\mathbf{f}_{c,v}$ and $\mathbf{H}$ from the given data, since precise knowledge of the camera and optics used to capture data is not widely available. The first step in this process will be to estimate the relative motion operators $\mathbf{M}$; we will consider a centralized registration operation, where the motions of all image data associated with a given location c are estimated with respect a fixed image. Once the motion estimates are available, the second step is to use a non-uniform interpolation (NUI) upsampling to generate blurry images with an upsampled datagrid. Finally, an alternative minimization approach is used to iteratively estimate the unknown blurs and high-resolution image data. The objective function used in the high resolution image estimation step will be modified to ensure that frames with error larger than a threshold will be labeled as an outlier and removed from the reconstruction process. This step will ensure that images from multiple source with potential errors in their metadata (such as GPS coordinates) will not degrade the final image quality. Prior to the image fusion, the metadata (if available) will be used to ensure that images with the largest difference in capture date will only be combined if their structural similarity [60] is smaller than a predefined threshold. This additional check ensures, for instance, that seasonal changes in vegetation data will not result in a blurring of the image resulting from the fusion/super-resolution process.

The choice of color space in which to compute the fused image data depends on the desired accuracy and the resulting computational tradeoffs. Our prior results [58] suggest that operating in the YUV space and primarily focusing on the Y components alone (and just resampling the U and V components) results in reasonable performance at much lower complexity that lends itself well to scaling for large data sets.

An important step in obtaining quantitative information from the processed image data is to calibrate the data to estimate dimensions of the various objects. We propose to use the dimensions of known objects in the scene to estimate the camera parameters and external (viewing) parameters of the calibration algorithm. The following standard relationship is used to quantify the relationship between the object in the 3D world and the observed 2D image. Specifically,

$$s\tilde{\mathbf{m}} = \mathbf{A}\begin{bmatrix}\mathbf{R} & \mathbf{t}\end{bmatrix}\tilde{\mathbf{M}}, \tag{8}$$

where s is an arbitrary scale factor, vector $\tilde{\mathbf{m}} = \begin{bmatrix}\mathbf{m} & 1\end{bmatrix}^T$, and extrinsic parameters $\begin{bmatrix}\mathbf{R} & \mathbf{t}\end{bmatrix}$ represent, respectively, the 3×3 rotation matrix and 3×1 translational vector from the world coordinate system to the camera coordinate system. The objective is to first estimate the *unknown* quantities $\mathbf{A}$, $\mathbf{R}$, and $\mathbf{t}$ using a set of objects with known dimensions and their corresponding image coordinates. Since the number of unknown quantities are fairly small (about 10 parameters typically) for a given imaging system, a few known dimensions are sufficient to ensure that we have an overdetermined system and use a maximum-likelihood estimator. Subsequently, the coordinates of any 2D point can be converted into their 3D world setting to obtain their estimated dimensions. This work is similar to other approaches that derive structure from motion (SfM) by solving for the unknown camera parameters and scene geometry [61]. Our group uses a similar process in a related work on health monitoring [62].

Image Attributes Extraction and Outlier Detection. Once the digital elevation models are derived from the multitude of visual data, they will become a part of the set of feature vectors used in classification. In addition, a large initial set of feature vectors will be used, including: pyramid of gradients, GCA feature vectors, and histograms of local binary patterns. Scene content classification will be undertaken to classify the outdoor images into a discrete number of classes. To ensure that the proposed classification is scalable, the number of classes will be adaptively modified using a process of pruning and sub-dividing.

Machine Learning with Geographical Features. Understanding the impact of contextual features on wireless performance has been an important prior contribution of our group. The key aspect of our work used a decision tree to form the relationshp between optimal, fine-resolution physical layer wireless parameters (such as modulation and coding rate) that maximizes throughput as a function of location, velocity and channel conditions [63]. A similar approach will be used here to understand the impact of topographical classification on quantitative wireless propogation. Further, as the size of our training sets increase, we will also consider the use of a convolutional neural network (CNN) to more directly obtain context information from the visual data.

LiDAR-based Propagation Isolation. We have mounted a RPLIDAR A2M6 laser scanner mounted on top of our existing drone communications platform, pictured in Figure 7(a). The A2M6 is a low-density laser scanner rotates 360 degrees in the horizontal plane and returns data pairs consisting of the angle in degrees of the scanner as well as the distance to the object from which the laser pulse reflected. In order to run and collect the data from the laser scanner, we also mounted a Raspberry Pi computer onto the drone and connected the scanner with a USB connection. To power the Raspberry Pi, and the laser scanner connected to it, we soldered a wire from the drones battery connector to a USB connection that plugged into the Raspberry Pi. The software to start the scanner was an application from the RPLIDAR SDK and was downloaded onto the Raspberry Pi. We first calibrated the LiDAR in a controlled indoor environment where we knew the dimensions.

For an initial outdoor experiment, we scanned a Shumard oak tree (Quercus shumardii) from four sides at stepped heights. Before flying, we measured four points around the tree, each orthogonal to each other and at a distance of 6.4 meters from the trunk of the tree. We then measured the circumference of the trunk to calculate its radius in order to determine the distance from a scan point to the center of the trunk and the relative position to the scan points. Once this preliminary data was collected, the drone scanning system was deployed at each of the four scan points. For each point, the drone was facing North and was flown to certain heights of 2, 4, 6, 8, and 10 meters for 10 seconds. In order to post-process the LiDAR data, we used the altitude readings from the drone flight logs to splice the data according to drone height. Once

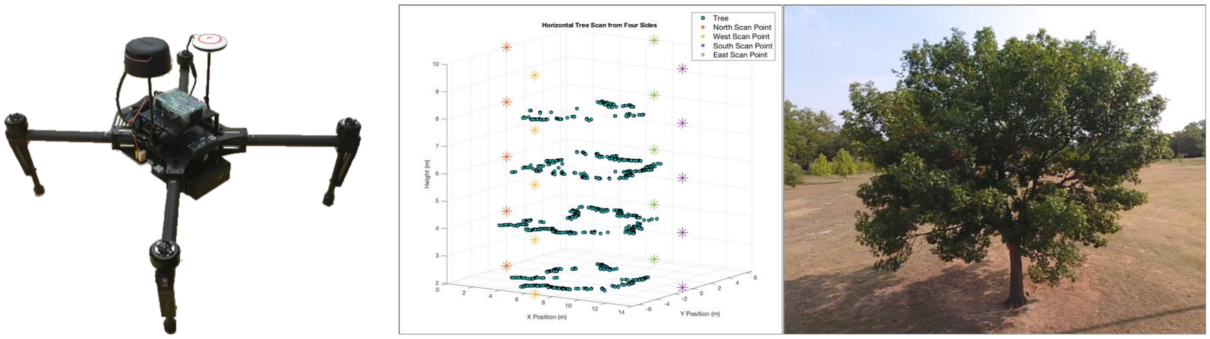

(a) Drone-Based LiDAR Platform. (b) 3D Scan of Tree.

Figure 7: LiDAR approach to isolate geographical feature density and propagation via experimentation.

all the LiDAR data was organized based on its location and height, we converted the angle and distance measurements into relative Cartesian coordinates. These points, plotted in a 3D scatter plot, represent the shape of the tree canopy at the aforementioned heights.

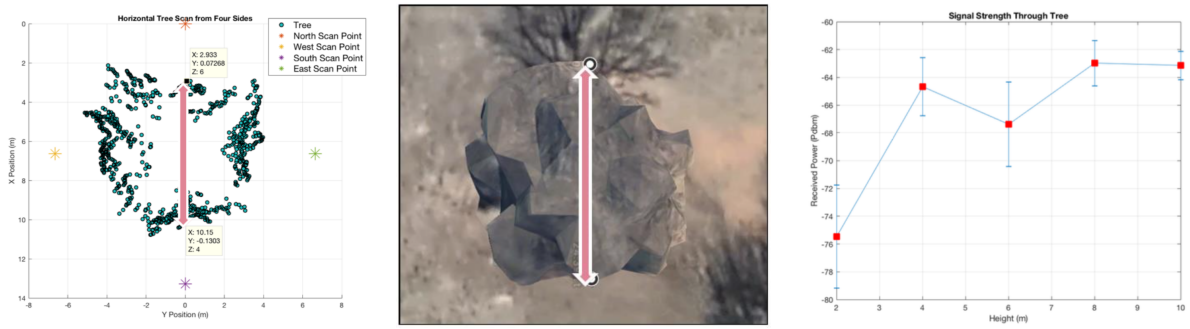

(a) LiDAR-based Tree Canopy (7.2 m). (b) Image-based Tree Canopy (7.4 m). (c) Wireless Propagation Through Tree.

Figure 8: Comparison in tree canopy from LiDAR- and image-based systems.

We now verify the inferred tree canopy via LiDAR (Figure 8(a)) against the satellite image of the same tree (Figure 8(b)). The LiDAR scan when used to estimate the diameter of the canopy was 97% accurate compared to satellite images. This is meaningful because it is proof that the scan was accurate, and because the size and shape of the canopy can be useful when related to wireless measurements. We then proceeded to measure the wireless propagation through the tree at the same heights as LiDAR measurements were captured by using a USRP E312 on two different drones positioned on opposite sides of the tree (North and South). We transmitted with a carrier frequency of 2.5 GHz with a gain of 17 dBm at the transmitter and a receive sampling rate of 32 kHz at the receiver. Both drones were flown above those respective points with their antennas facing each other and hovered in the same position for 60 seconds at each height. In Figure 8(c), we see that the larger tree canopy at the base of the tree results in far less signal through the tree, wheras the top of the tree has the highest received signal. We will perform extensive experiments through various tree and building types and sizes to understand the role of each geographical feature in the wireless propagation characteristics. We then will build an extensible measurement-driven model that combines our image-based and LiDAR-based local isolation of these factors to enable optimal topological formation in the following section.

Key Research Step: *We will explore the use of a deep convolutional neural network to develop the relationship between the attributes that are derived from the image data and the wireless characteristics that are observed in a given location. The wireless characteristics include the path loss in each frequency band that has been measured. An important attribute that will be studied is the long-term variation in propogation characteristics based on changes in vegetation (seasonal changes) or effect of additional urbanization. We*

plan to use an open-source tool such as TensorFlow [64] for training purposes.

4 Research Task 3: Multi-Dimensional Topological Formation of UAV Swarms

In this section, we consider how drones can be leveraged to *(i)* predict wireless propagation across multiple frequency bands (even if only one frequency band might be present on the drone for wireless measurement) and *(ii)* gather additional wireless data or images/video to address uncertainty in the propagation characteristics or geographical feature inference. Assuming we have some control over the placement of the drones (whether guiding crowdsourced drones through incentives or physical placement of our own drones), we could specifically target certain locations to address the uncertainty of our two techniques presented in the two previous sections. In particular, where might the best locations be to perform additional wireless spectrum measurements for propagation prediction and/or spectrum sensing applications and where would additional locations for images and videos be required and at what heights and angles?

4.1 Related Work

Unmanned aerial vehicles (UAVs) have been used for a number of applications such as disaster recovery [65], search and rescue [66], tracking and surveillance [67, 68], traffic monitoring [69–71], and many other military applications [72]. More specifically, there have been a number of works that use UAVs for the purpose of enhancing wireless networks for routing and ferrying [73], identifying increased spectral flux due to greater height [74], or challenges across the network stack [75, 76]. Moreover, Hayat et al. surveyed all air-to-air communication challenges for UAVs [77]. In contrast to these works, we seek to use drones for enhancement of our understanding of terrestrial networks and above-ground land features.

The majority of the work on radio propagation for drone communications has predominantly concentrated on simulation works without providing in-field experimental validation of simulation-based assumptions versus real geographical features and conditions [**?**, **?**, **?**, **?**]. For example, a channel fading model was proposed to predict the air-to-ground path loss in urban environments [**?**]. Simulations have also been conducted to investigate the impact of environmental attenuation on air-to-ground channels in the context of a High Altitude Platform (HAP) [**?**]. Other works have sought to maximize the radio coverage by optimizing the UAV position in urban environments [**?**]. System-level simulations also utilized path loss models to evaluate the performance of LTE and WiFi in aerial networks [**?**]. In-field experimentation has explored air-to-ground propagation to understand path loss and link performance [**?**, **?**, **?**]. However, most of these works focus on a specific environment type at a particular frequency band without varying the drone altitude or evaluating the effectiveness of multi-antenna beamforming systems in overcoming range and connectivity issues.

4.2 Preliminary Work

We have performed some initial experiments in the field for drone communications that motivate our problem of three-dimensional connectivity in airborne contexts. In particular, we have designed and printed mounts for an Ettus E312 (battery-powered 2x2 MIMO USRP) and two antennas (see above) to be secured on a DJI Matrice 100 (1 kg load capability). To do so, we have used a ROBO 3D printer and CAD software to ensure that a 10-cm separation exists between the two antennas for diversity purposes and allows repeatability in testing to position them in the same location. Fig. 9 depicts the drone communications platform. For a given experiment with a carrier frequency of 900 MHz and 1800 MHz, we mount two dual-band VERT900 omni-directional antennas, and for a given experiment at 5 GHz, we mount two dual-band VERT2450 antennas, which also operate in the 2.4 GHz band. Both antenna types provide a gain of 3 dBi. We have designed and implemented PHY and MAC layers that carry out IEEE 802.11-like channel feedback signaling using GNU Radio. The receiver configuration is matched for the USRP hardware, but is housed on a tripod at a height of 1 m above the ground. The received signals are amplified and down modulated to baseband. The digital samples are processed by GNU Radio blocks running on a Linux-based laptop.

In order to evaluate the drone-to-ground channel, we conduct downlink wideband experiments as a function of variable horizontal distances, drone hovering altitudes, and carrier frequencies. Based on the signal level at the receiver, we can calculate the path loss and shadowing standard deviation. Fig. 10(a)(b)(c) present the path loss of the three frequency bands after linearly fitting the mean values of path loss at each

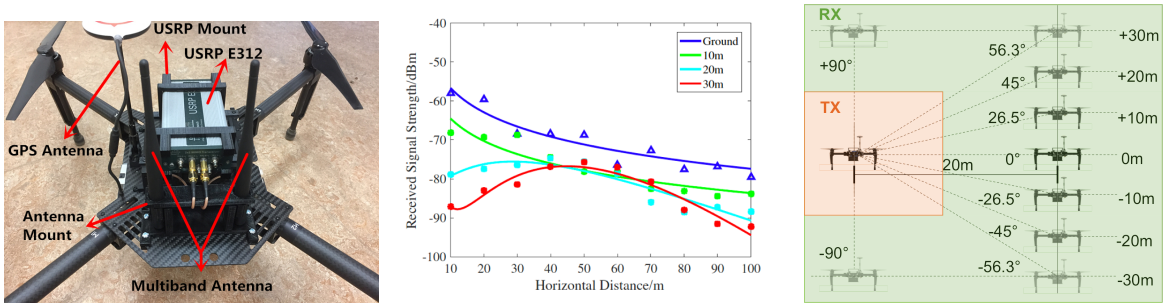

(a) Current UAV Comm. Platform. (b) Losses immediately below. (c) Drone-to-drone positions.

Figure 9: Equipment settings and setup for experiments. (a) Initial capabilities of UAV communications system. (b) Planned switching element for 3D communications. (c) NSF-funded multi-dimensional drone communications infrastructure consisting of UAVs and ceiling/ground massive MIMO control stations.

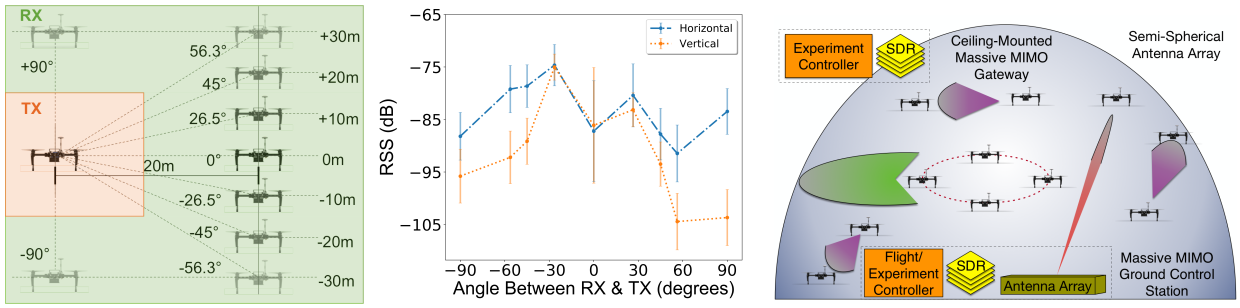

(a) Drone-to-drone positions. (b) Horizontal vs. vertical reception. (c) 3D Drone Infrastructure (MuDDI).

Figure 10: Measured Drone-to-Ground LoS Path Loss for different drone altitudes (ground, 10/20/30 m) and three different frequency bands: (a) 900 MHz, (b) 1800 MHz, and (c) 5 GHz.

horizontal distance and transmitter (drone) altitude. For carrier frequencies of 900 MHz and 1800 MHz, the signal reception seems to follow the expected pattern when the drone is on the ground and at 10-m altitude: the path loss increases as the distance increases at 10-m altitude. However, it is interesting to observe that the path loss decreases with distance at the shorter distances, and then increases from the minimum value at greater distances and at the higher altitudes. For example, 1800 MHz has an initial path loss value of 79 dB (at 10 m horizontal distance) when the drone altitude is 20 m, and then the path loss value decreases as the horizontal distance increases, reaching the minimum value of 70.4 dB at 40 m horizontal distance. This is due to the metal body of the drone that blocks the radio transmission at higher altitude and shorter horizontal distances and the omni-directional antenna pattern that better radiates at greater horizontal distances due to less obstruction.

4.3 Proposed Work

Key Research Steps: *There are several research steps that must be completed to further validate and extend these initial uncertainty findings: (i) Using this statistical learning framework, we will additionally explore the uncertainty related to small-scale fading prediction with respect to diverse geographical features. (ii) The initial analysis was performed with a land use tool [78] that relied on users to identify different geographical areas as having different classifications. In contrast, we will use our image-processing techniques to computationally map the geographical features to the wireless performance.*

5 Broader Impacts

Our project will expose engineering concepts to all age groups from under-represented minority kindergarteners to retirement-aged individuals both in person and through web-based videos. In addition, multiple SMU campuses will be leveraged to extensively involve undergraduate students in the research process as well as train undergraduate and graduate students through hands-on courses.

Undergraduate and Graduate Student Involvement. The PIs have designed a series of courses to equip undergraduate and graduate students alike to contribute to and learn from the crowdsourcing project. First and foremost, PI Camp will teach a course on the SMU-in-Taos campus each summer that will train undergraduate and graduate students to design novel measurement studies using mobile phones and drones on many of the concepts related to this extended white paper. Also, PI Camp teaches a senior-level undergraduate and graduate level course on the main SMU campus in which students learn to program Android and iOS devices. Students have a high degree of community engagement as the project topics often center on enhancements to the WiEye application and measurement infrastructure. PI Camp also teaches a course based on the WARP platform, enabling students to implement current physical and media access layers and form teams to study topics ranging from modulation rate adaptation and MAC design to context-awareness. The course incorporates inter-disciplinary topics of embedded programming, interrupt-driven operation, and FPGA-based design with wireless networking protocols. PI Rajan teaches a graduate course on applying optimization techniques in wireless networks, which is a project-based course that provides students with an opportunity to study the application of fundamental tools from optimization theory to solve large-scale wireless network problems. Lastly, PI Camp teaches a course on performance modeling in computer networks. Each of the PIs will include the knowledge gained from the research in future offerings of the courses.

Furthermore, the PIs will actively recruit undergraduate students from their course offerings to be actively involved with the research process in the form of smaller projects during normal semesters and larger projects during the summers or in senior-design projects. PI Camp and PI Rajan have collaborated on multiple NSF projects including a CRI grant for deploying an extensive context-aware measurement platform in the Dallas area. Multiple undergraduate researchers were involved with the development of the CRI infrastructure. Currently, the project team includes one female Ph.D. student and two undergraduate students to collaborate with five other Ph.D. students.

STEM Educational Outreach. The PI has received approval from the principal of a local elementary school (letter included), William Lipscomb Elementary, to form a monthly STEM Club where concepts and results will be shared to students from grades K-1 by undergraduate and graduate students on the project as well as the PI. Outside the scope of this extended white paper, the STEM Club will include biological and health related components, which will be led by the PI's wife, Mary Camp, MD. Lipscomb Elementary has an enrollment of over 87 percent Hispanic or African American with over 90 percent of the students qualifying as Low Socioeconomic Status (SES) [79]. Also, the Caruth Institute at SMU has agreed support this effort. For example, they have agreed to allow the use of their LEGO Mindstorm EV3 robots in the STEM Club to explore computer coding concepts and robotics. At the other end of the age spectrum, the SMU-in-Taos course that will be taught each summer will also interface with the predominantly-retired local community through evening seminars. Every Tuesday evening during the summer terms, 50-100 people attend seminars that are taught by SMU-in-Taos faculty. PI Camp will teach on the relevance of drones in modern engineering practices. Finally, PI Camp has already begun sharing drone-based videos from Taos with another SMU faculty, Troy Perkins, who is responsible for the promotional videos of the SMU-in-Taos facility. Dr. Perkins and Dr. Camp will work together each summer in Taos to provide instructional videos via web mediums on the use of mobile phones and drones in performing crowdsourcing, measurement study design, and in-situ experimentation.

6 Prior Federal Support

The following NSF projects have led up to the proposed research:

- CRI/II-New: Dallas-ARea Testbed for Context-Aware, Cognitive Research (DART-CARs) (CNS-0958436, $545,000, 03/01/10-02/28/13, Camp and Rajan were the PIs): The DART-CARs project

funded the equipment for development of an infrastructure for wireless measurements and protocol analysis in different environmental contexts. Campus buses, cars, and buildings were outfitted with radios and antennas from 400 MHz to 5.8 GHz with a channel emulator for repeatable experimentation of context-aware protocols [46, 63, 80–86].

- CAREER: Leveraging Simultaneous Access to Multiple Frequency Bands in Multihop Wireless Networks (CNS-1150215, $450,000, 02/15/12-01/31/17, Camp is the PI): Over the CAREER project, a crowdsourcing framework has been developed which has acquired over 250 million measurements of wireless signal strengths of cellular and WiFi networks. The key aspect of the project is studying the propagation and channel variability of different frequency bands in various environmental settings for the purpose of improving the performance of wireless networks of all types [46, 63, 82–85, 87–92].

- NeTS: Small: Channel Recognition for Optimized Links And Networks (CROLA) (CNS-1526269, $460,000, 9/15/15-8/31/18, Camp and Rajan are the PIs): The CROLA project allows channels to be both inferred from crowdsourced data and recognized from previously-observed channels for the purposes of optimizing link and network adaptation decisions via an online machine learning framework [63, 93].

- I-Corps: Efficient Terrain-Based Measurement Gathering for Path Loss Inference (IIP-1600549, $50,000, 12/15/15-5/31/16, Camp was the PI): The I-Corps project allowed us to refine our definition of the platform technology and expand the possible applications broadly through 100 customer discovery interviews. These discussions have led to multiple potential collaborations forming, including Samsung and AT&T.

Proposal Number	Short Name	2010	2011	2012	2013	2014	2015	2016	2017	2018
CNS-0958436	DART-CARs									
CNS-1150215	CAREER									
CNS-1526269	CROLA									
IIP-1600549	I-Corps									

Table 3: NSF projects which led to and will continue to develop the intellectual basis for this project.

Since wireless channel properties have long been known to be different based on the environmental characteristics [9, 10, 35] and devices are more aware of where they are than ever before, the DART-CARs project's primary objective was to build an infrastructure in and around the SMU campus where experimentation could be performed across various frequency bands from 400 MHz to 6 GHz simultaneously in diverse environmental contexts. The CAREER project has used and continue to use the DART-CARs testbed to evaluate the premise that wireless protocols could use knowledge of the environment to improve the performance of links and networks across various transmission rates and frequency bands. The CROLA project uses online learning to optimize link and network adaptation by inferring wireless channel properties when an environment has never been encountered before or recognizing a previously-observed channel.

Through the I-Corps project, we have shown that there is a direct correlation in terms of the complexity in the geographical features and the number of measurements it takes to accurately characterize these channel properties in a given region. The complexity problem and framework used can be used to quantify the uncertainty that a given number of measurements in a certain area would provide and allow comparison across areas for levels of uncertainty in propagation prediction for drone placement. In this extended white paper, we go one step further to completely rely on crowdsourced images and videos so that the relationship between geographical features and wireless propagation can be established and leveraged.

References

[1] A. Selyukh, "Faa expects 600,000 commercial drones in the air within a year," August 2016. [Online; posted 29-August-2016].

[2] Y. Naidoo, R. Stopforth, and G. Bright, "Development of an UAV for search and rescue applications," in *Proc. of IEEE Africon*, 2011.

[3] J. Zhao and J. Zhao, "Study on multi-UAV task clustering and task planning in cooperative reconnaissance," in *Proc. of IEEE Intelligent Human-Machine Systems and Cybernetics (IHMSC)*, 2014.

[4] "Facebooks solar drone to serve WiFi, stay aloft 90 days alpha model goes to museum." https://electrek.co/2017/12/08/facebook-solar-drone/, Dec. 2017.

[5] M. Mozaffari, W. Saad, M. Bennis, and M. Debbah, "Drone Small Cells in the Clouds: Design, Deployment and Performance Analysis," in *Proc. of IEEE Global Communications Conference*, 2015.

[6] S. Sekander, H. Tabassum, and E. Hossain, "Multi-tier Drone Architecture for 5G/B5G Cellular Networks: Challenges, Trends, and Prospects," *ArXiv e-prints*, Nov. 2017.

[7] L. Gupta, R. Jain, and G. Vaszkun, "Survey of important issues in UAV communication networks," *CoRR*, vol. abs/1603.08462, 2016.

[8] E. Yanmaz, M. Quaritsch, S. Yahyanejad, B. Rinner, H. Hellwagner, and C. Bettstetter, "Communication and coordination for drone networks," in *Ad Hoc Networks: 8th International Conference, ADHOCNETS 2016, Ottawa, Canada, September 26-27, 2016, Revised Selected Papers*, Springer International Publishing, 2017.

[9] T. S. Rappaport, *Wireless Communications, Principles and Practice*. Emerging Technologies, Upper Saddle River, New Jersey: Prentice Hall, 1996.

[10] G. L. Stuber, *Principles of Mobile Communication*. Boston: Kluwer, 4th ed., 2000.

[11] S. Ghassemzadeh, H. Worstell, and R. Miller, "Wireless neighborhood area network path loss characterization at 5.7 GHz," in *Proc. of IEEE VTC-Fall*, 2010.

[12] M. Hata, "Empirical formula for propagation loss in land mobile radio services," *Vehicular Technology, IEEE Transactions on*, vol. 29, no. 3, pp. 317–325, 1980.

[13] B. Hanci and I. Cavdar, "Mobile radio propagation measurements and tuning the path loss model in urban areas at GSM-900 band in istanbul-turkey," in *Proc. of IEEE VTC-Fall*, 2004.

[14] M. Akimoto, T. Shimizu, and M. Nakatsugawa, "Path loss estimation of 2 GHz and 5 GHz band FWA within 20 km in rural area," *Proc. of ISAP*, 2006.

[15] "Radio Mobile Website." http://www.cplus.org/rmw/english1.html, November 2016.

[16] "The world's biggest drone and video sharing platform." https://www.skypixel.com, Nov. 2016.

[17] A. Checco, C. Lancia, and D. J. Leith, "Using crowdsourcing for local topology discovery in wireless networks," *arXiv preprint arXiv:1401.1551*, 2014.

[18] J. Shi, Z. Guan, C. Qiao, T. Melodia, D. Koutsonikolas, and G. Challen, "Crowdsourcing access network spectrum allocation using smartphones," in *Proc. of ACM Hot Topics in Networks*, 2014.

[19] Y. Shavitt and E. Shir, "Dimes: Let the internet measure itself," *ACM SIGCOMM CCR*, vol. 35, no. 5, pp. 71–74, 2005.

[20] Z. S. Bischof, J. S. Otto, M. A. Sánchez, J. P. Rula, D. R. Choffnes, and F. E. Bustamante, "Crowdsourcing isp characterization to the network edge," in *Proc. of ACM SIGCOMM Measurements Up the Stack*, 2011.

[21] A. Rai, K. K. Chintalapudi, V. N. Padmanabhan, and R. Sen, "Zee: zero-effort crowdsourcing for indoor localization," in *Proc. of ACM MobiCom*, 2012.

[22] T. Hoßfeld, M. Seufert, M. Hirth, T. Zinner, P. Tran-Gia, and R. Schatz, "Quantification of youtube qoe via crowdsourcing," in *Proc. of IEEE Multimedia (ISM)*, 2011.

[23] M. Dischinger, M. Marcon, S. Guha, P. K. Gummadi, R. Mahajan, and S. Saroiu, "Glasnost: Enabling end users to detect traffic differentiation," in *Proc. of USENIX NSDI*, 2010.

[24] S. Yi, S. Chun, Y. Lee, S. Park, and S. Jung, *Radio Protocols for LTE and LTE-advanced*. John Wiley and Sons, 2012.

[25] J. M. Graybeal and K. Sridhar, "The evolution of SON to extended SON," *Bell Labs Technical Journal*, vol. 15, pp. 5–18, Dec. 2010.

[26] L. Ewe and H. Bakker, "Base station distributed handover optimization in LTE self-organizing networks," in *2011 IEEE 22nd International Symposium on Personal, Indoor and Mobile Radio Communications*, pp. 243–247, IEEE, 2011.

[27] J. Johansson, W. A. Hapsari, S. Kelley, and G. Bodog, "Minimization of drive tests in 3gpp release 11," *IEEE Communications Magazine*, vol. 50, no. 11, pp. 36–43, 2012.

[28] B. Gloss, J. Gebert, and Y. Quan, "Calibrating radio propagation models based on smartphone measurements for geo-aware cellular network self-optimization," in *2015 IEEE 81st Vehicular Technology Conference (VTC Spring)*, pp. 1–6, IEEE, 2015.

[29] M. Nakagami, "The m-distribution-a general formula of intensity distribution of rapid fading," *Statistical Method of Radio Propagation*, 1960.

[30] L. Rubio, N. Cardona, S. Flores, J. Reig, and L. Juan-Llácer, "The use of semi-deterministic propagation models for the prediction of the short-term fading statistics in mobile channels," in *IEEE VTC Fall*, 1999.

[31] M. D. Yacoub, J. E. V. Bautista, and L. G. de Rezende Guedes, "On higher order statistics of the nakagami-m distribution," *Vehicular Technology, IEEE Transactions on*, vol. 48, no. 3, pp. 790–794, 1999.

[32] M. Z. Win, G. Chrisikos, and J. H. Winters, "MRC performance for M-ary modulation in arbitrarily correlated Nakagami fading channels," *IEEE Communications Letters*, vol. 4, no. 10, pp. 301–303, 2000.

[33] V. Aalo, J. Zhang, *et al.*, "Performance analysis of maximal ratio combining in the presence of multiple equal-power cochannel interferers in a nakagami fading channel," *Vehicular Technology, IEEE Transactions on*, vol. 50, no. 2, pp. 497–503, 2001.

[34] T. S. Rappaport *et al.*, *Wireless communications: principles and practice*, vol. 2. Prentice Hall, 1996.

[35] J. Friis, "A note on a simple transmission formula," *Proceedings of the IRE*, vol. 34, pp. 254–256, May 1946.

[36] J. W. Mckown and R. L. Hamilton, "Ray tracing as a design tool for radio networks," *IEEE Network Magazine*, pp. 27–30, Nov. 1991.

[37] K. Rizk, J. F. Wagen, and F. Gardiol, "Two-dimensional ray-tracing modeling for propagation prediction in microcellular environments," *IEEE Transactions on Vehicular Technology*, vol. VT-46, pp. 508–518, May 1997.

[38] Y. Okumura, E. Ohmori, T. Kawano, and K. Fukuda, "Field strength and its variability in vhf and uhf land-mobile radio service," *Rev. Elec. Commun. Lab*, vol. 16, no. 9, pp. 825–73, 1968.

[39] E. Östlin, H.-J. Zepernick, and H. Suzuki, "Macrocell path-loss prediction using artificial neural networks," *IEEE Transactions on Vehicular Technology*, vol. 59, no. 6, pp. 2735–2747, 2010.

[40] K. Stocker and F. Landstorfer, "Empirical prediction of radiowave propagation by neural network simulator," *Electronics letters*, vol. 28, no. 8, pp. 724–726, 1992.

[41] I. Popescu, D. Nikitopoulos, P. Constantinou, and I. Nafornita, "ANN prediction models for outdoor environment," in *2006 IEEE 17th International Symposium on Personal, Indoor and Mobile Radio Communications*, pp. 1–5, IEEE, 2006.

[42] Z. Stankovic, B. Milovanovic, M. Veljkovic, and A. Dordevic, "The hybrid-neural empirical model for the electromagnetic field level prediction in urban environments," in *Neural Network Applications in Electrical Engineering, 2004. NEUREL 2004. 2004 7th Seminar on*, pp. 189–192, IEEE, 2004.

[43] A. Neskovic, N. Neskovic, and D. Paunovic, "Indoor electric field level prediction model based on the artificial neural networks," *IEEE Communications Letters*, vol. 4, no. 6, pp. 190–192, 2000.

[44] P. Petrus, J. H. Reed, and T. S. Rappaport, "Geometrical-based statistical macrocell channel model for mobile environments," *IEEE Transactions on Communications*, vol. 50, no. 3, pp. 495–502, 2002.

[45] E. Östlin, H. Suzuki, and H.-J. Zepernick, "Evaluation of the propagation model recommendation itu-r p. 1546 for mobile services in rural australia," *IEEE Transactions on Vehicular Technology*, vol. 57, no. 1, pp. 38–51, 2008.

[46] H. Liu, J. He, D. Rajan, and J. Camp, "Outlier detection for training-based adaptive protocols," in *Proc. of IEEE WCNC: MAC*, (Shanghai, China), Apr. 2013.

[47] H. Tong and C. Lin, "Non-negative residual matrix factorization with application to graph anomaly detection," in *Proc. of SDM*, 2011.

[48] Y. She and A. Owen, "Outlier detection using nonconvex penalized regression," *Journal of the American Statistical Association*, vol. 106, no. 494, pp. 626–639, 2011.

[49] A. Katartzis and H. Sahli, "A stochastic framework for the identification of building rooftops using a single remote sensing image," *IEEE Transactions on Geoscience and Remote Sensing*, vol. 46, pp. 259–271, Jan. 2008.

[50] A. Ö. Ok, "Robust detection of buildings from a single color aerial image," in *GEOgraphic-Object-Based Image Analysis (GEOBIA)*, 2008.

[51] C. Wu, "VisualSFM : A visual structure from motion system," Nov. 2016.

[52] L.-C. Chen, T.-A. Teo, Y.-C. Shao, Y.-C. Lai, and J.-Y. Rau, "Fusion of LiDAR data and optical imagery for building modeling," *International Archives of the Photogrammetry, Remote Sensing and Spatial Information Sciences*, vol. 35, no. B4, pp. 732–737.

[53] "Cataloging public objects using aerial and street-level images urban trees," in *IEEE Conference on Computer Vision and Pattern Recognition (CVPR)*, 2016.

[54] T. O. Olasupo, C. E. Otero, K. O. Olasupo, and I. Kostanic, "Empirical path loss models for wireless sensor network deployments in short and tall natural grass environments," *IEEE Transactions on Antennas and Propagation*, vol. 64, pp. 4012–4021, Sept 2016.

[55] C. E. Otero, R. Haber, A. M. Peter, A. AlSayyari, and I. Kostanic, "A wireless sensor networks' analytics system for predicting performance in on-demand deployments," *IEEE Systems Journal*, vol. 9, pp. 1344–1353, Dec 2015.

[56] R. Haber, A. Peter, C. E. Otero, I. Kostanic, and A. Ejnioui, "A support vector machine for terrain classification in on-demand deployments of wireless sensor networks," in *Systems Conference (SysCon), 2013 IEEE International*, pp. 841–846, April 2013.

[57] E. Faramarzi, D. Rajan, and M. P. Christensen, "Unified blind method for multi-image super-resolution and single/multi-image blur deconvolution," *IEEE Transactions on Image Processing*, vol. 22, pp. 2101–2114, June 2013.

[58] E. Faramarzi, D. Rajan, F. C. A. Fernandes, and M. P. Christensen, "Blind super resolution of real-life video sequences," *IEEE Transactions on Image Processing*, vol. 25, pp. 1544–1555, April 2016.

[59] Z. Zhang, "A flexible new technique for camera calibration," *IEEE Transactions on Pattern Analysis and Machine Intelligence*, vol. 22, pp. 1330–1334, Nov 2000.

[60] Z. Wang, A. C. Bovik, H. R. Sheikh, and E. P. Simoncelli, "Image quality assessment: from error visibility to structural similarity," *IEEE Transactions on Image Processing*, vol. 13, pp. 600–612, April 2004.

[61] M. Westoby, J. Brasington, N. Glasser, M. Hambrey, and J. Reynolds, "structure-from-motion photogrammetry: A low-cost, effective tool for geoscience applications," *Geomorphology*, vol. 179, pp. 300 – 314, 2012.

[62] *Masters Thesis, Southern Methodist University*, 2016.

[63] H. Liu, J. He, O. Altintas, R. Vuyyuru, J. Camp, and D. Rajan, "FIT: On-the-fly, in-situ training with sensor data for SNR-based rate selection," in *Proc. of IEEE WCNC*, (New Orleans, Louisiana), Mar. 2015.

[64] "Tensorflow - an open source software library for machine intelligence." http://www.tensorflow.org, Nov. 2016.

[65] G. Tuna, B. Nefzi, and G. Conte, "Unmanned aerial vehicle-aided communications system for disaster recovery," *Journal of Network and Computer Applications*, vol. 41, pp. 27–36, 2014.

[66] J. Adams, C. Humphrey, M. Goodrich, J. Cooper, B. Morse, C. Engh, and N. Rasmussen, "Cognitive task analysis for developing unmanned aerial vehicle wilderness search support," *Journal of Cognitive Engineering and Decision Making*, vol. 3, no. 1, pp. 1–26, 2009.

[67] A. Jaimes, S. Kota, and J. Gomez, "An approach to surveillance an area using swarm of fixed wing and quad-rotor unmanned aerial vehicles uav(s)," in *IEEE international conference on system of systems engineering (SoSE)*, 2008.

[68] S. Kota and M. Jamshidi, "ATS: aerial tracking and surveillance system," in *IEEE International conference on system of systems engineering (SoSE)*, 2008.

[69] S. Srinivasan, H. Latchman, J. Shea, T. Wong, and J. McNair, "Airborne traffic surveillance systems: video surveillance of highway traffic," in *ACM second international workshop on video surveillance and sensor networks*, 2004.

[70] A. Puri, "A survey of unmanned aerial vehicles (UAV) for traffic surveillance," 2005.

[71] M. Kafi, Y. Challal, D. Djenouri, M. Doudou, A. Bouabdallah, and N. Badache, "A study of wireless sensor networks for urban traffic monitoring: applications and architectures," *Procedia Computer Science*, vol. 19, pp. 617–626, 2013.

[72] D. Glade, "Unmanned aerial vehicles: implications for military operations," Tech. Rep. DTIC document, 2000.

[73] M. Asadpour, B. V. den Bergh, D. Giustiniano, K. A. Hummel, S. Pollin, and B. Plattner, "Micro aerial vehicle networks: An experimental analysis of challenges and opportunities," *IEEE Communications Magazine*, vol. 52, pp. 141–149, July 2014.

[74] M. J. Marcus, "Spectrum policy challenges of uav/drones," *IEEE Wireless Communications*, vol. 21, pp. 8–9, Oct. 2014.

[75] B.-N. Cheng, F. J. Block, B. R. Hamilton, D. R. C. Timmerman, L. Veytser, and A. Narula-Tam, "Design considerations for next-generation airborne tactical networks," *IEEE Communications Magazine*, vol. 52, pp. 138–145, May 2014.

[76] Y. Saleem, M. H. Rehmani, and S. Zeadally, "Integration of cognitive radio technology with unmanned aerial vehicles: Issues, opportunities, and future research challenges," *Journal of Network and Computer Applications*, vol. 50, pp. 15–31, 2014.

[77] S. Hayat, E. Yanmaz, and R. Muzaffar, "Survey on unmanned aerial vehicle networks for civil applications: A communications viewpoint," *IEEE Communications Surveys and Tutorials*, vol. PP, 2016.

[78] "Open Street Map." www.openstreetmap.org, November 2016. License: http://www.openstreetmap.org/copyright.

[79] "William Lipscomb Elementary School Profile." https://goo.gl/H6dnLu, Nov. 2016.

[80] J. Camp, O. Altintas, R. Vuyyuru, and D. Rajan, "Context-aware collection, decision, and distribution (C2D2) engine for multi-dimensional adaptation in vehicular networks," in *Proc. of ACM VANET Workshop*, (Las Vegas, NV), Sept. 2011.

[81] J. He, H. Liu, P. Cui, J. Landon, O. Altintas, R. Vuyyuru, D. Rajan, and J. Camp, "Design and experimentation of context-aware link-level adaptation," in *Proc. of IEEE INFOCOM*, (Miami, FL), Mar. 2012.

[82] R. Meikle and J. Camp, "A global measurement study of context-based propagation and user mobility," in *Proc. of the 4th ACM international workshop on Hot topics in planet-scale measurement (ACM HotPlanet)*, (Low Wood Bay, Lake District, UK), June 2012.

[83] P. Huang, M. Tonnemacher, Y. Du, D. Rajan, and J. Camp, "Towards scalable network emulation: Channel accuracy versus implementation resources," in *Proc. of IEEE INFOCOM 2013*, (Turin, Italy), Apr. 2013.

[84] P. Huang, D. Rajan, and J. Camp, "Weibull and suzuki fading channel generator design to reduce hardware resources," in *Proc. of IEEE WCNC: PHY*, (Shanghai, China), Apr. 2013.

[85] P. Cui, H. Liu, J. He, O. Altintas, R. Vuyyuru, D. Rajan, and J. Camp, "Leveraging diverse propagation and context for Multi-Modal vehicular applications," in *Proc. of IEEE VTC WIVEC*, (Dresden, Germany), June 2013.

[86] D. R. Pengfei Cui, Hui Liu and J. Camp, "A measurement study of white spaces across diverse population densities," *IEEE 10th WiNMeE*, 2014.

[87] Y. Du, E. Aryafar, J. Camp, and M. Chiang, "iBeam: Intelligent client-side multi-user beamforming in wireless networks," in *Proc. of IEEE INFOCOM*, (Toronto, Canada), Apr. 2014.

[88] Y. Du, D. Rajan, and J. Camp, "Analysis and experimental evaluation of rate adaptation with transmit buffer information," *EURASIP Journal on Wireless Communications and Networking*, vol. 62, pp. 1–14, Apr. 2014.

[89] P. Cui, H. Liu, D. Rajan, and J. Camp, "A measurement study of white spaces across diverse population densities," in *Proc. of IEEE WiOpt 2014 (WiNMeE Workshop-The 10th International Workshop on Wireless Network Measurements and Experimentation)*, (Hammamet, Tunisia), May 2014.

[90] P. Cui, M. Tonnemacher, D. Rajan, and J. Camp, "WhiteCell: Energy-efficient use of unlicensed frequency bands for cellular offloading," in *Proc. of IEEE DySPAN*, (Stockholm, Sweden), Oct. 2015.

[91] Y. Shi and J. Camp, "Downlink resource allocation for enhanced inter-cell interference coordination (eICIC) in heterogeneous cellular networks," *In International Journal of Enhanced Research in Science, Technology & En gineering*, vol. 5, no. 2, pp. 45–53, 2016.

[92] P. Cui, Y. Dong, H. Liu, D. Rajan, E. Olinick, and J. Camp, "WhiteMesh: Leveraging White Spaces in wireless mesh networks," in *Proc. of IEEE WiOpt (WiNMeE Workshop-The 12th International Workshop on Wireless Network Measurements and Experimentation–Invited)*, (Tempe, Arizona), May 2016.

[93] J. He, H. Liu, P. Cui, J. Landon, D. Rajan, and J. Camp, "Geometry-based channel recognition for context-aware applications," in *Proc. of IEEE WiOpt (WiNMeE Workshop-The 12th International Workshop on Wireless Network Measurements and Experimentation–Invited)*, (Tempe, Arizona), May 2016.